



A comprehensive kinetic model for Cu catalyzed liquid phase glycerol hydrogenolysis

Tapas Rajkhowa, Guy B. Marin, Joris W. Thybaut*

Laboratory for Chemical Technology, Ghent University, Technologiepark 914, B-9052 Ghent, Belgium



ARTICLE INFO

Article history:

Received 5 August 2016

Received in revised form 8 December 2016

Accepted 17 December 2016

Available online 21 December 2016

Keywords:

Glycerol

Propylene glycol

Copper

Hydrogenolysis

Kinetics

ABSTRACT

Hydrogenolysis of biomass-derived glycerol has been investigated as an alternative route for the production of value-added chemicals, such as 1,2-propanediol, also commonly denoted as propylene glycol (PG). Intrinsic glycerol hydrogenolysis kinetics have been acquired experimentally on a stable, commercial copper-based catalyst in an isothermal trickle-bed reactor at 463–513 K, hydrogen pressures from 6.5 to 8 MPa and space times (W/F_G^0) from 25 to 340 kg s mol⁻¹ resulting in glycerol/PG conversions from 1 to 75 mol%. The selectivity to PG amounts to at least 90%. For a given conversion, the lowest selectivity is observed at the highest temperature. Glycerol is predominantly dehydrated to acetol which is subsequently converted to PG. Co-feeding reaction products, *i.e.*, PG and water, does not affect the rate of glycerol conversion. Additionally, glycerol can lead to minor side reactions forming products such as 1,3-propanediol, ethylene glycol while PG can degrade to ethanol, methanol and propanol. A comprehensive kinetic model accounting not only for the formation of main reaction products but also of side products was constructed. The activation energy of the rate-determining step for glycerol dehydration towards acetol was estimated at 84 kJ mol⁻¹, exceeding that of the rate-determining step of the consecutive hydrogenation into PG by about 25 kJ mol⁻¹. The high selectivity towards PG is attributed to (1) the relatively lower surface reaction rates for the parallel and the consecutive side reactions and (2) its low affinity for adsorption on the catalyst surface compared to glycerol at the investigated experimental conditions.

© 2016 The Author(s). Published by Elsevier B.V. This is an open access article under the CC BY-NC-ND license (<http://creativecommons.org/licenses/by-nc-nd/4.0/>).

1. Introduction

Growing concerns about global climate change and the diminishing fossil reserves have been important driving factors for the development of technologies starting from renewable biomass resources instead of traditional petroleum [1,2]. In this regard the implementation of fatty acid methyl esters (biodiesel) as an automotive fuel has been gaining prominence, especially in the US and Europe. While biodiesel is more expensive to produce than petroleum-derived diesel, the former's renewable nature and lower emissions have encouraged governments around the world to subsidize its production [3]. The energy policies around climate change are anticipated to further enhance the demand for bio-fuels in the short and long term [4]. These factors have thus lead to a widespread increase in the biodiesel production in the past decade and, as a corollary, to an over supply of the by-product glycerol. The latter is unavoidably produced with a yield of about 10%wt of the biodiesel, resulting in a decline in its price. The current price

for the highest quality glycerol is about \$1100/metric ton and that for lower grades between \$180–\$540/metric ton [5]. Consequently, one way to increase the sustainability and profitability of a biodiesel plant is to investigate potential new applications of glycerol as low-cost feedstock for functional derivatives or as a precursor of high value fine chemicals. This is even more relevant in the current scenario with sub \$40 per barrel oil prices, which increases the price difference between petroleum-derived diesel and biodiesel even further [6].

Glycerol valorization can be achieved through various routes [7]. An effective pathway to this purpose is situated in the production of chemicals which are conventionally derived from fossil resources through the petrochemical industry, hence, replacing a currently non-renewable production route with one which is renewable, environmentally friendly and potentially carbon neutral. Propane-1,2-diol (propylene glycol) is an example of such a non-toxic added-value chemical with applications in cosmetics, pharmaceuticals, polyester resins, de-icing, *etc.* It is conventionally produced through propylene oxide hydration, the latter being obtained from petroleum derived propylene [8]. However, an interesting alternative route is through the catalytic hydrogenolysis of glycerol.

* Corresponding author.

E-mail address: Joris.Thybaut@UGent.be (J.W. Thybaut).

Nomenclature

Roman symbols

a_i	activity for component i (-)
C_t	total concentration of active sites ($\text{mol kg}_{\text{cat}}^{-1}$)
cn	carbon number (-)
E_a	activation energy (kJ mol^{-1})
E_r	relative experimental error for response i corresponding to a 95% confidence level (-)
F_i	molar flow rate of component i (mol s^{-1})
f_i	fugacity for component i (MPa)
h	Planck constant (J s)
k_B	Boltzmann constant (J K^{-1})
K_i	equilibrium coefficient (reaction dependent)
k_i	rate coefficient (s^{-1})
L	molar flow rate in liquid phase (mol s^{-1})
n_{exp}	number of experiments (-)
n_p	number of parameters (-)
n_{rep}	number repeat experiments (-)
n_{resp}	number of responses (-)
p_t	total pressure (MPa)
R	universal gas constant ($\text{J K}^{-1} \text{mol}^{-1}$)
R_i	net rate of formation of component i ($\text{mol s}^{-1} \text{kg}_{\text{cat}}^{-1}$)
S	selectivity (-)
T	temperature (K)
V	molar flow rate in vapor phase (mol s^{-1})
w_j	weighing factor of response j during regression (-)
X	conversion (-)
x_i	mole fraction of i in liquid phase (-)
Y	yield (-)
y_i	mole fraction of i in vapor phase (-)
ΔG^0	standard Gibbs energy (kJ mol^{-1})
ΔH^0	standard enthalpy change (kJ mol^{-1})
ΔS^0	standard entropy change ($\text{kJ mol}^{-1} \text{K}^{-1}$)
W	catalyst mass (kg)
SSQ	residuals sum of squares (-)

Greek symbols

β	model parameter
μ_i	chemical potential of component i (J mol^{-1})
ϕ	fugacity coefficient (-)
θ_i	fractional site coverage of component i (-)

Superscripts

\wedge	model calculated
l	liquid phase
v	vapor phase

Subscripts

A	acetol
G	glycerol
i, j	components
PG	propylene glycol

In the past few years, glycerol hydrogenolysis has been investigated extensively [9–18] in both gas and liquid phase. Investigations thus far have been performed towards developing the process [18] and effective catalysts [9–12]. Transition and noble metals have been dealt with, Cu, Ru and Ni being most popular [19–21]. Although the activity of the noble metal catalysts was found to exceed that of the transition metals, the selectivity towards side products such as 1,3-propanediol and ethylene glycol was reported to be higher on the former compared to the latter [11]. Among transition metals, Ru catalysts exhibit a lower

selectivity towards propylene glycol due to more pronounced C–C bond scissions, hence, yielding more ethylene glycol and gaseous by-products as compared to Cu based catalysts [13]. The latter are known for their selective C–O bond scission performance [14] and, hence, exhibit a superior performance in terms of selectivity towards propylene glycol.

Depending on the catalyst and the operating conditions used, glycerol hydrogenolysis can proceed through two principle mechanisms: a dehydration–hydrogenation mechanism occurs with 1-hydroxyacetone (acetol) as the intermediate [18,15] and a dehydrogenation–dehydration–hydrogenation reaction with 2,3-dihydroxy-propanal (glyceraldehyde) as the intermediate [14,10]. Acetol being observed as an intermediate in the presence of Cu-based catalysts such as copper-silica [16] and copper-alumina [17] supports the former, *i.e.*, the dehydration–hydrogenation mechanism. A bi-functional route has been suggested by various authors with the dehydration step catalyzed by acid sites (usually from the support) and hydrogenation catalyzed by the metal [22,15,23]. However, among other things based on a widely reported linear relation between the active Cu surface area and hydrogenolysis activity [17,16,24–26], the unique role of metallic copper in promoting both glycerol dehydration and hydrogenation has been generally accepted.

Although glycerol hydrogenolysis has received significant research interest in the past decade, few studies have been performed on understanding the detailed kinetics of the reaction. Liquid phase experiments have been preferred for kinetic studies. Lahr and Shanks [27] developed a Langmuir–Hinshelwood type model for kinetics acquired on a commercial Ru/C catalyst and indicated the importance of the competitive adsorption of the main reaction products. However, the model did not explicitly account for the intermediate reaction steps and, hence, could not provide adequate mechanistic insights. Zhou et al. [28] derived a Langmuir–Hinshelwood type model over a Cu-ZnO-Al₂O₃ catalyst using a fixed-bed tubular reactor. Essential features of this model were the slow nature of the glycerol dehydration towards acetol and the weak adsorption of propylene glycol. Torres et al. [29] derived power law rate equations to quantify the relative importance of the side reactions over a bimetallic Ru-Re catalyst. Finally, Vasilidiou and Lemonidou [16] derived power law kinetics over a Cu-SiO₂ catalyst using a batch reactor based on the dehydration–hydrogenation mechanism. A weak PG formation rate on the glycerol concentration and a first order dependence of hydrogen concentration was reported.

The present work aims at investigating the liquid phase glycerol hydrogenolysis kinetics over a stable, commercial Cu based catalyst in a fixed bed tubular reactor. Intrinsic kinetic experiments have been performed by varying operating conditions such as temperature, hydrogen pressure and feed concentration at different space times, W/F_G^0 in order to investigate their effect on the catalytic performance. Based on the experimental observations an intrinsic kinetic model is developed, aiming at a quantified understanding of the catalytic chemistry both for the main and the side products in a wider range of operating conditions, including feedstock composition.

2. Procedures

2.1. Catalyst and materials

Commercial glycerol and propylene glycol with 99.5% purity was used. 99.99% nitrogen and hydrogen were obtained from Air-Liquide. A commercial, Cu based catalyst on an inert support was used which exhibited the following typical properties: BET surface area of $60 \text{ m}^2 \text{ g}^{-1}$, Cu particle diameter of 10 nm, Cu surface

Table 1
Operating conditions employed during the experimental program.

Parameter	Range
T, K	463–513
p, MPa	6.5–8.0
W/F _G ⁰ , kg s mol ⁻¹	25–350
X, mol%	1–75
Feed	Glycerol PG Co-feeding mixture ^a

^a 8.5, 48 and 43.5 mol% glycerol, PG and H₂O.

area of 10 m² g⁻¹ and a total concentration of active sites, C_t, of 1 mmol kg⁻¹.

2.2. Set-up and operating conditions

All experiments were performed in a high-throughput kinetics mechanistic investigation setup [30,31] comprising 8 parallel fixed-bed tubular reactors operated in three phase flow condition within the trickle flow regime for the present investigation. The liquid was fed to the reactor from a pre-heated glass reservoir, 323 K, with an Eldex Optos high pressure liquid metering pump. A flash drum, situated downstream of the back pressure regulator, operated at ambient temperature is used to separate the gas from the liquid.

Catalyst particles with a diameter between 500 and 700 μm were used for the experiments. Prior to its loading in the reactor, the catalyst was diluted with an amount twice that of the catalyst mass of α-Al₂O₃ particles of 150 μm diameter. Diluent particles that were significantly smaller compared to the catalyst particles were used to further ensure effective catalyst wetting and improved hydrodynamics as per the recommendations from Sie and Krishna [32] and Al-Dahhan and Dudukovic [33]. The α-Al₂O₃ dilution particles were determined to be inert towards glycerol dehydration and/or hydrogenolysis through blank tests performed at the operating conditions reported in Table 1.

Once loaded, the catalyst was dried in a nitrogen flow of 30 NL/h and kept at a temperature of 473 K and pressure of 0.5 MPa for about 6 h. The catalyst was then reduced at the same temperature and pressure by increasing the hydrogen partial pressure from 0 to 100%. The hydrogen flow was increased in increments of 5 NL/h with 30 min time intervals between each increment while reducing the nitrogen flow by the same amount until a hydrogen flow of 30 NL/h was obtained. Finally, the 30 NL/h hydrogen flow was maintained for 3 h at the same temperature and pressure before setting the reactor to the desired operating temperature and pressure.

An overview of the operating conditions is given in Table 1. The liquid products were analyzed using an Agilent 6850 gas chromatograph equipped with a DB-1 capillary column (60 m × 0.25 μm × 0.25 μm) and a flame ionization detector (FID). The calibration factors of the different components were determined by means of a multi point calibration using a broad range of calibration mixtures. n-Butanol procured from Sigma-Aldrich was used as the dilution solvent for the sample analysis. Gaseous products analyzed using an Agilent 3000 micro gas chromatograph composed mainly of hydrogen and had negligible contribution to the carbon balance. The mass balance was verified via electronic weighing of the feed as well as the effluent recipient. The carbon balance was closed up to 100 ± 2% for all the reported data.

Steady state operation was reached at every experimental condition. This was verified through consecutive analysis of the liquid products every two to three hours and the measurement was considered 'acquired' after at least three consecutive analyses showing less than 2% deviation. Only then operating conditions were adopted to those of the next experiment. When testing several reaction conditions on a single catalyst batch, a back check

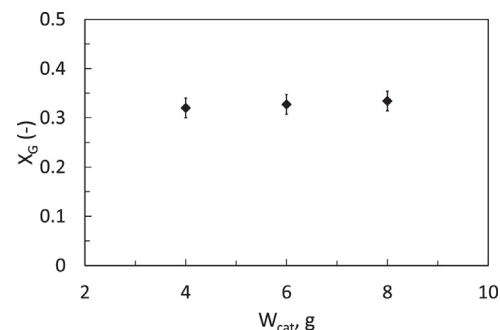


Fig. 1. Glycerol conversion as a function of catalyst mass, W, at constant W/F_G⁰, T = 503 K, p = 6.5 MPa, W/F_G⁰ = 40 kg s mol⁻¹, F_{H₂}⁰/F_G⁰ = 5.

at a reference condition was performed at regular intervals. During these experiments negligible deactivation, i.e., less than a 5% relative decrease in activity was observed. Typically, maximum 7 experimental conditions were tested with a single catalyst loading.

2.3. Data treatment

The conversion of a feed component k, X_k, is defined on a molar basis as shown in Eq. (1)

$$X_k = \frac{F_k^0 - F_k}{F_k^0} \quad (1)$$

F_k⁰ and F_k represent the inlet and outlet molar flow rates of component k. The selectivity for product i, S_i, coming from the feed component k, is calculated using Eq. (2) where cn_i is the number of carbon atoms in component i.

$$S_i = \frac{cn_i F_i}{cn_k (F_k^0 - F_k)} \quad (2)$$

The yield of the various products is defined by Eq. (3):

$$Y_i = \frac{cn_i F_i}{cn_k F_k^0} = S_i X_k \quad (3)$$

The error bars represent the experimental error, Er, on a variable V (e.g., conversion) determined from repeat experiments and is calculated using Eq. (4) where n_{rep} is the number of repeat experiments, V_{avg} the average of the variable and V_i its value for ith experiment.

$$Er = \frac{1.96}{V_{avg}} \sqrt{\frac{1}{n_{rep} - 1}} \quad (4)$$

2.4. Intrinsic kinetics regime verification

In order to measure intrinsic kinetics, the experimental data have to be free from mass and heat transfer effects [34]. In this regard, the hydrodynamics and catalyst wetting efficiency also play an important role and need to be assessed. The presence of external mass transfer limitations can be experimentally assessed by systematically increasing the catalyst loading (W) while keeping the space time (W/F_G⁰), the time required to process one reactor volume of the feed at inlet conditions, constant. In the absence of external mass transfer limitations, the conversion should be independent of the catalyst mass. This assessment is typically performed at the highest operating temperature to maximize the reaction rate and, hence, the probability of a transport limited regime. Experiments performed at a temperature of 503 K, 6.5 MPa, F_{H₂}⁰/F_G⁰ of 5 show a constant conversion, see Fig. 1.

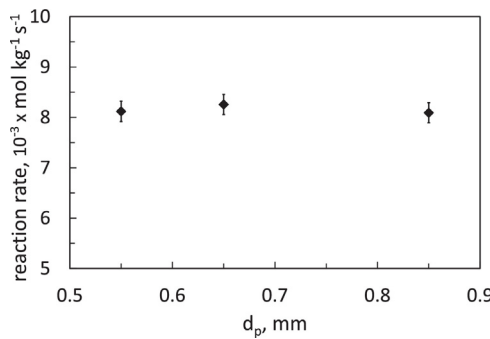


Fig. 2. Reaction rate as a function of catalyst pellet diameter, d_p , at constant W/F_G^0 , $T = 503\text{ K}$, $p = 6.5\text{ MPa}$, $W/F_G^0 = 40\text{ kg s mol}^{-1}$, $F_{H_2}^0/F_G^0 = 5$.

The occurrence of internal mass transfer limitations can be experimentally investigated by varying the catalyst pellet diameter and measuring the reaction rates. In the absence of internal diffusion limitations, the reaction rate should remain constant as a function of the catalyst pellet diameter. The experiments performed at identical conditions of T , p , W/F_G^0 , $F_{H_2}^0/F_G^0$ and conversion (Fig. 2) show identical reaction rates as a function of particle diameter such that it can be concluded that there are no internal mass transfer limitations.

Ng [35] provided correlations for the calculation of the minimal superficial gas mass flux, G , at a given superficial liquid mass flux, L , for the transition between various flow regimes. As compared to the maximum superficial mass flux amounting to $0.02\text{ kg m}^{-2}\text{ s}^{-1}$ as used in our work, those for the transition from trickling to spray flow and from trickling to pulsing were calculated to be $19\text{ kg m}^{-2}\text{ s}^{-1}$ and $6\text{ kg m}^{-2}\text{ s}^{-1}$ respectively, thus confirming the trickle flow regime. The most critical wetting number, W , calculated for the operating conditions used in this work amounted to 8×10^{-5} compared to a minimum value of 5×10^{-6} for obtaining even irrigation and complete wetting suggested by Gierman [36] and Sie [37], thus confirming complete wetting.

In addition to experimental validation, mass and heat transfer gradients were also evaluated at the extreme operating conditions using criteria related to the phenomena relevant for trickle flow [34,38,39]. As pure hydrogen was used for the experiments mass transfer limitations at the gas side are considered to be negligible. Mass transfer at the liquid side of the gas–liquid interphase and at the liquid–solid interphase were assessed by calculating the Carberry number [34,38]. The most critical value obtained for the Carberry number corresponds to H_2 mass transfer from the gas to liquid and amounted to 0.046, which is just below the limit of 0.05. The intraparticle diffusion limitation was assessed with the Weisz–Prater criterion [39]. The effectiveness factor for both hydrogen and glycerol was close to unity with the most critical Weisz modulus (Φ) value amounting to 0.015 for hydrogen, which is sufficiently below the limit value of 0.08.

Heat transfer effects were assessed by the criteria reported by Mears [40]. At the highest temperature *i.e.*, 503 K, the interparticle, interphase and intraparticle temperature gradients are found to be 0.85, 0.09 and 0.003 K respectively. These gradients are smaller than the value of the criteria for less than 5% deviation in the observed rate as suggested by Mears, *i.e.*, 1 K [40].

2.5. Thermodynamic non-ideality at liquid phase condition and vapor liquid equilibrium

Chemical reaction rates depend on thermodynamic activities or fugacities of reactants and products especially in non-ideal gas–liquid–solid reaction systems. Concentrations may only be

used for ideal mixtures or under special conditions as discussed by Madon and Iglesia [41]. The basis for the calculation of these non-idealities can be established with the help of the definition of chemical potential μ_i , represented by Eq. (5).

$$\mu_i = \mu_i^0 + RT \ln a_i \quad (5)$$

where μ_i^0 represents the chemical potential at the standard state and a_i the thermodynamic activity of component i . In this work, the activity coefficient is determined via the group additivity method UNIFAC [42].

To account for the solubility of the gas *i.e.*, hydrogen, in the liquid phase the vapor–liquid equilibrium is solved using the PSRK [43,44] equation of state. The necessary condition for equilibrium is the equality of chemical potentials, which, in case identical standard states have been selected for the different phases considered, leads to equality of thermodynamic activities or fugacities [45].

$$f_i^l = f_i^v \quad (6)$$

with f_i representing the fugacity of component i and the superscripts v, l referring to the vapor and the liquid phase respectively. Expanding and rearranging Eq. (6) in terms of “equilibrium ratio”, K_i^v and the mole fractions of i in vapor, y_i and in liquid, x_i leads to the following equation:

$$K_i^v = \frac{y_i}{x_i} = \frac{\phi_i^l}{\phi_i^v} \quad (7)$$

if equations of state are used for both phases, with ϕ_i representing the fugacity coefficient of component i . A mass balance for phase splitting, Eq. (8), can then be solved iteratively to determine the fraction of component i in both the phases, complimented by the constraint that the mole fractions in each phase sum to unity.

$$Fz_i = Vy_i + Lx_i \quad (8)$$

with F the total molar flow rate, V the molar flow rate in the vapor phase and L the molar flow rate in the liquid phase.

2.6. Reactor model

Since, the experiments have been performed in a plug flow reactor and are free of transport limitations at the pellet scale, a 1-dimensional, isothermal and pseudo-homogeneous reactor model could be used.

$$\frac{dF_i}{dW} = R_i \quad (9)$$

with

$$W = 0, \quad F_k = F_k^0 \quad (10)$$

as the initial condition. W being the catalyst mass, F_i the molar flow rate of component i and R_i the net rate of formation component i . The net rates, R_i , are computed with the liquid phase concentrations, calculated by solving the vapor–liquid equilibrium using the procedure discussed in Section 2.5. The integration is done using an open source code *i.e.*, DASPK, which is a differential algebraic equation solver available from netlib [46].

2.7. Parameter estimation procedure

The methodology for parameter estimation is based on the minimisation of the weighted sum of squares, SSQ , of the residuals between the experimental, $F_{i,j}$, and model calculated, $\hat{F}_{i,j}$, outlet molar flow rates and, hence, by maximizing the posteriori probability of the experimental error in the acquired data. This occurs by adjusting the model parameter vector, b , which is expected to

Table 2

Conversion and product selectivities (%) with pure glycerol feed at different temperatures and space times with $p = 8$ MPa and $F_{H_2}^0/F_G^0 = 5$.

	473	483	493	503
T, K	473	483	493	503
$W/F_G^0, \text{kg s mol}^{-1}$	213	157	74	87
$X_G, \%$	26	37	31	77
Acetol	2.78	4.21	6.07	1.28
PG	94.4	93.2	92.4	94.7
Ethylene glycol	0.89	0.34	0.24	0.35
Methanol	0.72	0.33	0.42	1.15
Ethanol	0.12	0.27	0.36	0.59
Propionic acid	0.00	0.45	0.10	0.51
1,3-Propanediol	0.50	0.48	0.27	0.43
1-Propanol	0.86	0.00	0.05	0.43
2-Propanol	0.10	0.65	0.15	0.53

approach the real parameter vector β at the minimum of the following objective function:

$$SSQ = \sum_{i=1}^{n_{\text{exp}}} \sum_{j=1}^{n_{\text{resp}}} w_j (F_{i,j} - \hat{F}_{i,j})^2 \xrightarrow{b} \text{Min} \quad (11)$$

with n_{exp} the number of experiments, n_{resp} the number of responses and w_j is the weighing factor for response j . The latter is calculated from the covariance matrix of the experimental errors (see Eq. (12)). A total of 55 experiments with 10 responses (all reactants and products except H_2 and H_2O , see Table 2 for the products) were used for the regression.

$$w_j = \frac{1}{\sigma_{jj}^2} = \left[\frac{\sum_{i=1}^{n_{\text{exp}}} (F_{i,j} - \hat{F}_{i,j})^2}{n_{\text{exp}} \cdot n_{\text{resp}} - n_p} \right]^{-1} \quad (12)$$

A two stage parameter estimation is performed by use of a Rosenbrock algorithm [47] followed by a Levenberg–Marquardt algorithm [48]. An in-house developed code for the former, which is more robust against divergence than the latter, is used in the first stage to bring the parameter values in the neighborhood of the optimal parameter values [47]. Subsequently the more advanced Levenberg–Marquardt algorithm, implemented as ODRPACK 2.01 obtained from netlib, takes over and ensures a quadratic convergence to the optimal estimates [48]. Additional code was added to the ODRPACK to retrieve statistical information, such as t -value, F -value, etc., for the model and the model parameters.

The regression results are evaluated on a statistical basis. The physical significance of the model as a whole is tested by the calculation of the ratio of the mean regression sum of squares and the mean residual sum of squares (Eq. (13)), i.e., the so-called F test for the global significance of the regression. The regression is considered to be globally significant when the calculated F value exceeds the tabulated F one, with n_p and $n_{\text{exp}} \cdot n_{\text{resp}} - n_p$ degrees of freedom.

$$F = \frac{\frac{\sum_{i=1}^{n_{\text{exp}}} \sum_{j=1}^{n_{\text{resp}}} w_j \hat{F}_{i,j}^2}{n_p}}{\frac{\sum_{i=1}^{n_{\text{exp}}} \sum_{j=1}^{n_{\text{resp}}} w_j (F_{i,j} - \hat{F}_{i,j})^2}{n_{\text{exp}} \cdot n_{\text{resp}} - n_p}} > F_{n_p, n_{\text{exp}} \cdot n_{\text{resp}} - n_p} \quad (13)$$

The t value for parameter i is calculated as the ratio of the difference between the estimated b_i and the postulated value b_i^* , i.e., 0, and its corresponding standard deviation (Eq. (14)). A parameter estimate is considered significantly different from b_i^* , c.q., 0, at a certain confidence level, e.g., 95%, when the calculated t value exceeds the tabulated t value with $n_{\text{exp}} \cdot n_{\text{resp}} - n_p$ degrees of freedom at that confidence level.

$$t = \frac{b_i}{\sqrt{V(b_i)_{i,j}}} > t_{n_{\text{exp}}(n_{\text{resp}} - n_p)} \quad (14)$$

The model performance can be visualized by means of a parity diagram, where the model calculated values are plotted on the y -axis against the experimental values on the x -axis. In order to formally ‘accept’ the model, the model calculated values should approach the experimental values as much as possible, i.e., approaching as much as possible the first bisector. A normal distribution of the model calculated values around the bisector is expected due to the assumed normal distribution of the experimental error.

3. Experimental results and kinetic model development

3.1. Effect of operating conditions on glycerol hydrogenolysis and reaction network construction

Table 2 shows the glycerol hydrogenolysis products as obtained on the industrial Cu based catalyst which included acetol, propylene glycol (PG), ethane-1,2-diol (ethylene glycol), methanol, ethanol, propanoic acid (propionic acid), propane-1,3-diol (1,3-propanediol), propan-1-ol (1-propanol) and propan-2-ol (2-propanol). PG selectivities exceeding 90% are achieved over a wide range of glycerol conversions with acetol being the second most abundant product with selectivities from 1 to 6%. The selectivities towards the other products are typically below 1%, even at a higher glycerol conversion of 77%, see Table 2.

Fig. 3a shows that as the conversion increases, the selectivity towards the desired product, PG, also increases and the acetol selectivity decreases. Fig. 3a is analogous to a first-rank delplot, which allows separation of primary from nonprimary products [49]. Finite intercepts for acetol in the first-rank delplot and that for PG in the second-rank delplot (see Fig. 3b) indicate the primary nature of the former and the secondary nature of the latter. The high PG observed selectivities, even at low glycerol conversion, indicate that the consecutive formation of PG from acetol occurs on a much smaller time scale than that of acetol formation.

Increasing the temperature while keeping the pressure, space time and $F_{H_2}^0/F_G^0$ constant leads to an increase in glycerol conversion as shown in Fig. 4a. This expected increase is due to the increase in the reaction rate with temperature. The assessment of the temperature effect on the product distribution was performed at iso conversion in order to eliminate any conversion effect from the temperature effect. Fig. 4b shows the selectivities towards PG and acetol at iso glycerol conversion of about 0.35. A decrease in PG selectivity and an increase in acetol selectivity are observed with increasing temperature. This trend can be attributed to a higher activation energy of the reaction leading to acetol from glycerol thus leading to a more pronounced increase in its reaction rate with temperature as compared to that for the production of propylene glycol.

No significant pressure effect on the reaction rate was observed in the range from 6.5 to 8.0 MPa, see Fig. 5. The catalyst being totally wetted by the liquid in the trickle bed reactor, the pressure can only impact on the H_2 solubility. In the range of pressures used in this work these solubility differences are marginal.

A recycling mode can be used to minimize the heat effects related to the exothermicity of the reaction. This scenario can be experimentally assessed by using a glycerol feed diluted with PG and water. A liquid mixture of 70, 15 and 15 wt% of PG, glycerol and water respectively, which corresponds to a molar ratio of 0.48:0.085:0.435, was used to investigate the effects of the major reaction products on the conversion. The kinetic experiments performed with this diluted glycerol stream as feed to the reactor exhibited a space time effect only, see Fig. 6. This indicates strong glycerol adsorption on the catalyst surface as compared to water and PG.

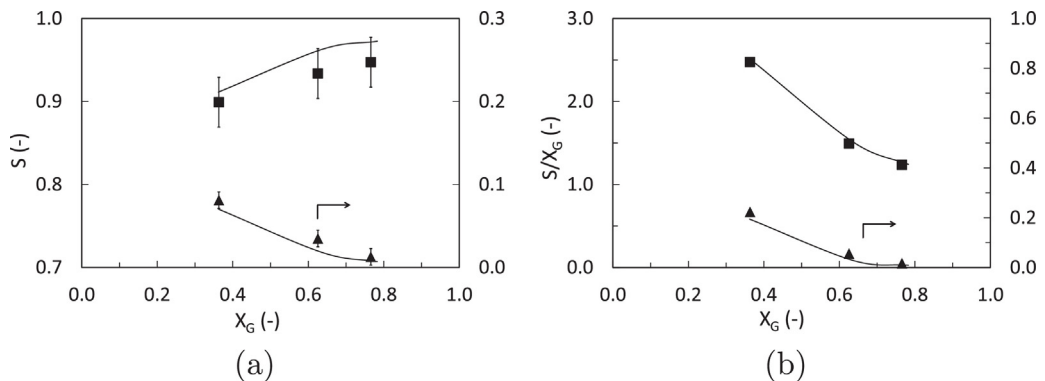


Fig. 3. Responses as a function of glycerol conversion at $T = 503\text{ K}$, $p = 7\text{ MPa}$, $F_{H_2}^0/F_G^0 = 5$, first rank delplot (a), second-rank delplot (b). (■) PG; (▲) acetol. Full lines were calculated using model simulated outlet flow rates from reactor model Eq. (9) along with rate equations Eq. (15)–(25) and the parameter estimates from Table 5.

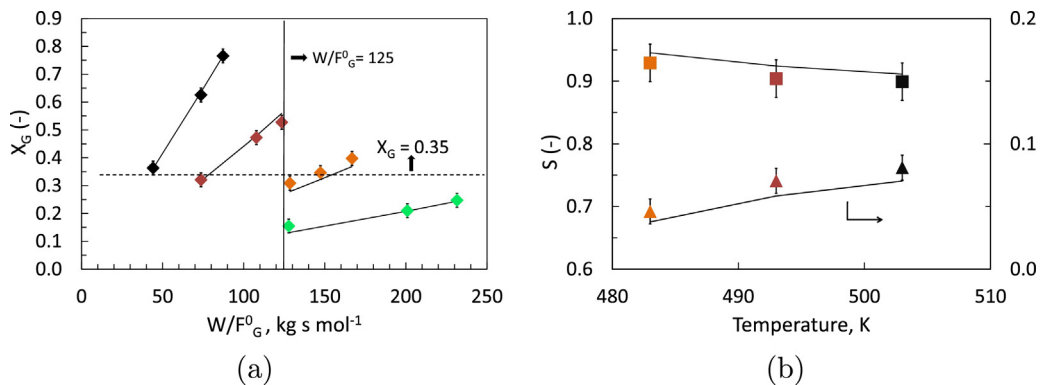


Fig. 4. Glycerol conversion (a) and product selectivity at $X_G = 0.35$ (b) as a function of W/F_G^0 and temperature at $p = 7.5\text{ MPa}$, $F_{H_2}^0/F_G^0 = 5$. (◆) conversion; (■) PG; (▲) acetol; (◆) 503 K; (◆) 493 K; (◆) 483 K; (◆) 483 K; (◆) 473 K. Full lines were calculated using model simulated outlet flow rates from reactor model Eq. (9) along with rate Eqs. (15)–(25) and the parameter estimates from Table 5.

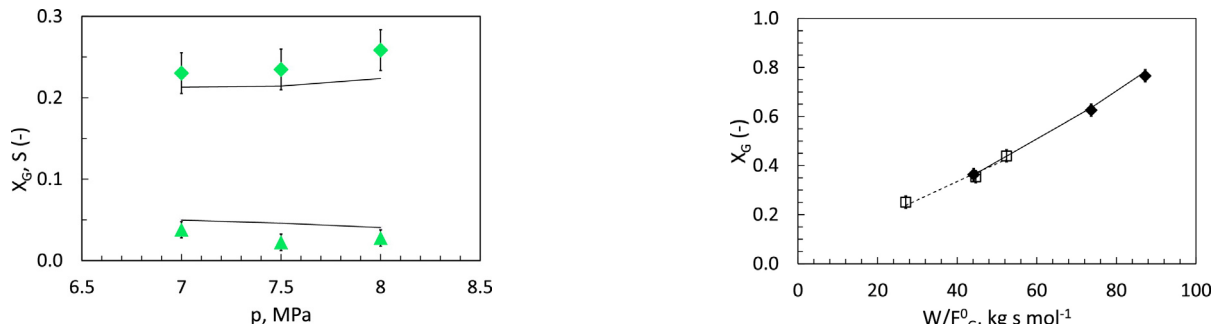


Fig. 5. Glycerol conversion and acetol selectivity as a function of pressure at $F_{H_2}^0/F_G^0 = 5$, $T = 473\text{ K}$, $W/F_G^0 = 210\text{ kg s mol}^{-1}$. (◆) conversion; (▲) acetol selectivity. Full lines were calculated using model simulated outlet flow rates from reactor model Eq. (9) along with rate Eq. (15)–(25) and the parameter estimates from Table 5.

In order to quantitatively investigate the consecutive reactions of PG, pure PG was used as feed. Experiments at different temperatures, pressures, hydrogen to PG molar ratios and space time show an extremely low PG conversion at similar conditions as used for pure glycerol, viz Table 3. The products obtained in these experiments predominantly were acetol, 1-propanol and 2-propanol with very small amounts of propionic acid, ethanol and methanol. Non-zero intercepts for propionic acid, ethanol and 1-propanol in the second rank delplot indicate the secondary nature of these products with respect to glycerol, see Fig. 7b. Since, the conversion of acetol towards PG is fast, ethanol and 1-propanol originating from PG manifest themselves as secondary products. Additionally, a second rank delplot, see Fig. 7b, also indicates the non-secondary nature of

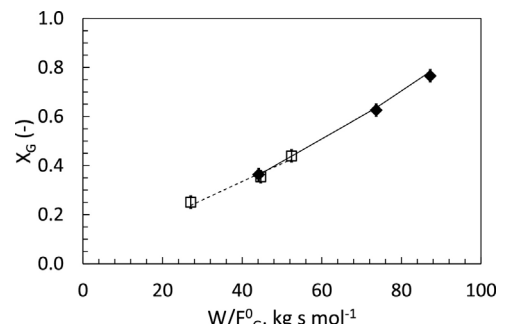


Fig. 6. Glycerol conversion as a function of W/F_G^0 at $T = 503\text{ K}$, $p = 8\text{ MPa}$, $F_{H_2}^0/F_G^0 = 0$ with (◆) pure glycerol as feed and (□) 0.48:0.085:0.435 molar fraction of PG:glycerol:water as feed. Lines were calculated using model simulated outlet flow rates from reactor model Eq. (9) along with rate Eqs. (15)–(25) and the parameter estimates from Table 5. (—) pure glycerol and (---) diluted glycerol.

Table 3

Conversion and product selectivities (%) with pure PG as feed at different temperatures, pressures and space times.

$T, \text{ K}$	483	483	493	503
$W/F_{PG}^0, \text{ kg s mol}^{-1}$	34	46	43	21
$p, \text{ MPa}$	75	70	75	65
$F_{H_2}^0/F_{PG}^0$	1.6	3.6	2.0	2.0
$X_{PG}, \%$	1.5	1.2	2.1	1.7
Acetol	62.51	47.73	50.34	68.30
Methanol	0.51	0.63	0.47	0.64
Ethanol	3.66	4.89	5.12	2.88
Propionic acid	3.33	4.83	5.16	2.79
1-Propanol	11.75	16.09	14.93	9.35
2-Propanol	18.23	25.86	24.00	16.03

methanol and 2-propanol. A similar investigation, but at gas phase conditions and in the absence of hydrogen, by Sato et al. [17] with propylene glycol on Cu-Al₂O₃ also resulted in a high selectivity towards acetol with small amounts of propionic acid, 2-propanone, acetaldehyde and acetic acid. The latter two components were not detected in the present work. In the presence of hydrogen, 2-propanone is expected to rapidly form 2-propanol through a hydrogenation reaction. 1-Propanol is proposed to be formed from PG through a similar dehydration-hydrogenation mechanism with propanal as intermediate. Direct hydrogenolysis of PG is also possible and leads to the formation of ethanol and methanol. Finally, isomerization of acetol leads to the formation of a secondary product, propionic acid.

The finite intercept for ethylene glycol and 1,3-propanediol in the first rank and the second rank deplot respectively, see Fig. 7, clearly indicate the primary nature of the former and the secondary nature of the latter. Thus, based on a comparison of Tables 2 and 3 it can be concluded that in addition to forming acetol via dehydration, glycerol can also be dehydrated to 3-hydroxypropionaldehyde (HPA) or form ethylene glycol and methanol through hydrogenolysis. The quantitative analysis, not only of the main reaction products but also the by-products, during glycerol hydrogenolysis in a wide range of operating, as discussed above, leads to the reaction network represented in Fig. 8. A similar reaction network was also suggested by Gandarias et al. for glycerol hydrogenolysis and degradation reaction over a Pt over amorphous silica alumina catalyst in an aqueous liquid phase [23].

3.2. Rate equations

The kinetic modeling of glycerol hydrogenolysis is based on the data discussed in Section 3.1. The dominating PG and acetol selectivities (Table 2) indicate the importance of the glycerol dehydration and acetol hydrogenation reaction steps in the product distribution. Therefore, this section aims in the first instance at the development of a detailed kinetics scheme for these two steps, also denoted as the main kinetics.

Based on a linear relation between active Cu surface area and hydrogenolysis activity [26,17,50], see also Section 1, a mechanism occurring exclusively on the copper phase is proposed, the role of the support being limited to providing sufficient surface area for the deposition of the active phase and preventing its sintering. Although supports such as SiO₂ and γ-Al₂O₃ contain weak acid sites, no evidence for any correlation between their acid strength and catalytic activity could be established. Moreover, the added value of a dual site mechanism (not further discussed in the current work) in terms of more adequately reproducing the experimental results, was considered not to outweigh the additional effort in terms of number of model parameters to be determined. A similar lack of incentives in terms of model performance by increasing the complexity of a kinetic model has also been reported for aromatic hydrogenation [51,52].

Table 4 presents the catalytic cycles and the overall reactions, for the production of acetol from glycerol and its subsequent hydrogenation to PG, considered in the current work according to the Horiuti/Temkin format [53]. H₂ adsorbs dissociatively on the copper surface and competes with the associative adsorption of reactant glycerol as well as of the reaction products acetol, propylene glycol, water and partially hydrogenated acetol, AH, for the production of PG. The concentrations of adsorbed methanol, ethanol, ethylene glycol, propionic acid, 1,3-propanediol, 1-propanol and 2-propanol were considered sufficiently low such that they could be neglected, see also Table 2. The adsorption steps are considered to be quasi-equilibrated. The glycerol dehydration (e4) is considered to be rate determining for the production of acetol while the second hydrogenation step (e6) is considered to be

Table 4

Elementary steps and corresponding Horiuti numbers (σ) in the catalytic cycles constituting the overall reactions considered for the main kinetics.

		σ_I	σ_{II}	
$G + * \rightleftharpoons G*$	(K_G)	1	0	(e1)
$H_2 + 2* \rightleftharpoons 2H*$	(K_H)	0	1	(e2)
$A + * \rightleftharpoons A*$	(K_A)	-1	1	(e3)
$G^* + * \rightleftharpoons A^* + H_2O^*$	(k_1, K_1)	1	0	(e4)
$A^* + H^* \rightleftharpoons AH + *$	(K_{AH})	0	1	(e5)
$AH + H^* \rightleftharpoons PG^* + *$	(k_2, K_2)	0	1	(e6)
$PG + * \rightleftharpoons PG*$	(K_{PG})	0	-1	(e6)
$H_2O + * \rightleftharpoons H_2O^*$	(K_{H_2O})	-1	0	(e7)
$G \rightleftharpoons A + H_2O$	(K^0)			
$A + H_2 \rightleftharpoons PG$	(K^b_2)			

* – active site, G – glycerol, H – hydrogen, A – acetol, PG – propylene glycol.

the rate-determining step for the production of propylene glycol. The latter agrees with the reported first order dependence of the PG production on hydrogen [16,29]. The resulting rate equations are:

$$r_1 = C_t^2 k_1 \left(\theta_* \theta_{G*} - \frac{1}{K_1} \theta_{A*} \theta_{H_2O*} \right) \quad (15)$$

$$r_2 = C_t^2 k_2 \left(\theta_{AH*} \theta_{H*} - \frac{1}{K_2} \theta_{PG*} \theta_* \right) \quad (16)$$

with C_t the total concentration of active sites, k_1 , k_2 the rate coefficients, K_1 , K_2 equilibrium coefficients for the rate-determining surface reaction, θ_* the fractional coverage of free sites and θ_i the surface coverages of surface species i . The subscripts for rate, r , and the rate coefficient, k , are in line with the label of the overall reaction in Fig. 8, leading to the formation of the corresponding component. For reasons of thermodynamic consistency, r_1 , was included in the model as a potentially reversible reaction as it belongs to the main reaction route. For the byproduct formation no thermodynamic consistency was specifically implemented. Given the relative amounts of main products formed compared to by-products, reverse reactions, if at all, are expected to occur among the main reactions. From the equilibrium relations corresponding to reaction steps (e1)–(e3), (e7) and (e8) the surface coverages of the adsorbed species can be calculated according to Eqs. (17) and (18):

$$\theta_{i*} = \theta_* K_i a_i \quad (17)$$

$$\theta_{H*} = \theta_* \sqrt{K_H} \quad (18)$$

with i representing all the surface species except hydrogen. The site balance is shown in Eq. (19):

$$\theta_* + \theta_{H*} + \theta_{G*} + \theta_{A*} + \theta_{PG*} + \theta_{AH*} = 1 \quad (19)$$

Eqs. (9) and (15)–(19) describe the main kinetics for glycerol hydrogenolysis.

The carbon–carbon bond scissions in glycerol and propylene glycol leading to ethylene glycol, methanol and ethanol are assumed to proceed via a two step hydrogenation. The rate-determining step is assumed to correspond to the second hydrogenation step, similar to reaction steps (e5) and (e6), but now with the further hydrogenated surface species GH^* and PGH^* as reactant.

$$r_3 = C_t^2 k_3 \theta_{PGH*} \theta_{H*} \quad (20)$$

$$r_4 = C_t^2 k_4 \theta_{GH*} \theta_{H*} \quad (21)$$

The production of 1,3-propanediol, 1-propanol and 2-propanol is assumed to proceed via a dehydration-hydrogenation mechanism through 3-hydroxy-propionaldehyde (HPA), propanal and 2-propanone intermediates respectively as shown in the reaction network in Fig. 8. In the presence of H₂ these intermediates

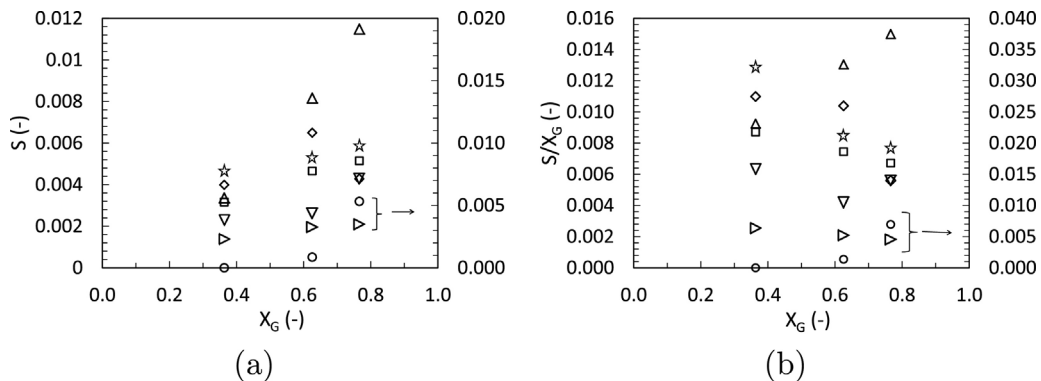


Fig. 7. Responses (side products) as a function of glycerol conversion at $T=503\text{ K}$, $p=7\text{ MPa}$, $F_{\text{H}_2}^0/F_G^0=5$, first rank delplot (a), second-rank delplot (b). (◆) 1,3-propanediol; (▷) ethylene glycol; (□) propionic acid; (★) ethanol; (△) methanol; (▽) 1-propanol; (○) 2-propanol.

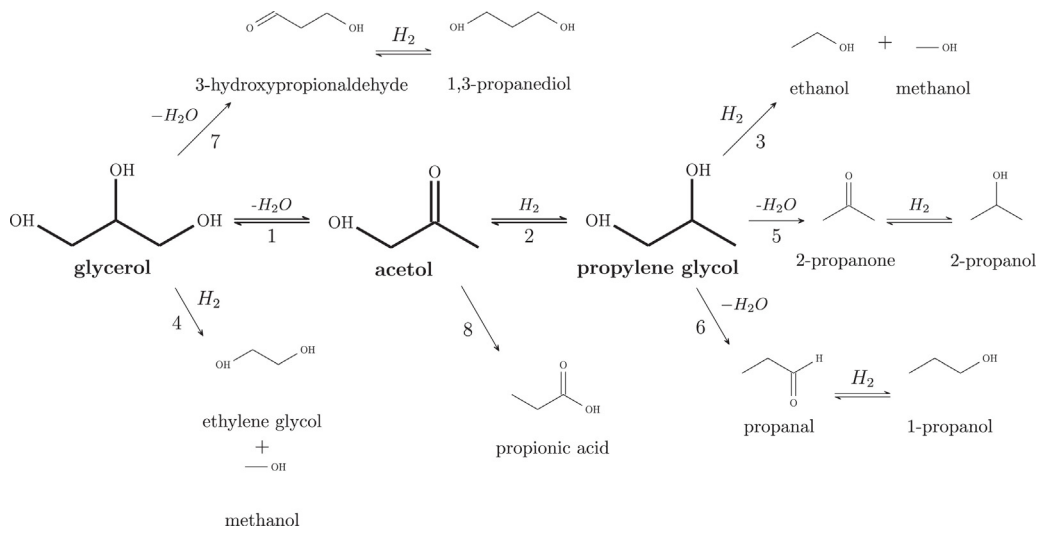


Fig. 8. Comprehensive reaction network for glycerol hydrogenolysis.

are converted quasi-instantaneously. Hence, the formation of 1,3-propanediol from glycerol and 1-propanol and 2-propanol from PG can be modeled assuming the dehydration step to be rate-determining. As the adsorption steps are considered quasi-equilibrated, this results in following rate equations:

$$r_5 = C_t^2 k_5 \theta_{PG*} \theta_* \quad (22)$$

$$r_6 = C_t^2 k_6 \theta_{PG*} \theta_* \quad (23)$$

$$r_7 = C_t^2 k_7 \theta_{G*} \theta_* \quad (24)$$

Finally, propionic acid is considered to be produced through acetol isomerization involving the same type of active sites. Hence, this leads to the following rate equation:

$$r_8 = C_t k_8 \theta_{A*} \quad (25)$$

3.3. Parameter estimation

Sixteen coefficients are involved in the model constructed in the previous section: eight rate coefficients ($k_1 - k_8$), three surface reaction equilibrium coefficients (K_1 , K_2 , K_{AH}) and five chemisorption coefficients (K_G , K_A , K_{PG} , K_{H_2} and K_{H_2O}). The temperature dependence of the rate coefficients and the chemisorption coefficients are given by Eqs. (26) and (27).

$$K_i = \exp\left(\frac{\Delta S_i^0}{R}\right) \exp\left(-\frac{\Delta H_i^0}{RT}\right) \quad (26)$$

$$k_i = A_i \exp\left(-\frac{E_{ai}}{RT}\right) \quad (27)$$

with A_i the pre-exponential factor, E_{ai} the activation energy, ΔS^0 the change in entropy due to adsorption/reaction and ΔH^0 the adsorption/reaction enthalpy. Hence, for applying the model to non-isothermal conditions 32 parameters have to be determined, which exceeds the number that can reasonably be obtained via model regression to experimental data. Hence, well justified values will be selected for a selection of model parameters, while the remaining ones will be estimated by regression of the complete experimental data set.

In order to reduce the number of parameters to be estimated via regression, the pre-exponential factors, A_i , and the adsorption entropy, ΔS^0 , are calculated a priori based on statistical thermodynamics.

The first term in Eq. (26) is calculated using the change in entropy due to adsorption by relating the adsorption entropy to a loss of translational degrees of freedom, approximated via gas phase translational entropy through the Sackur-Tetrode equation [54]. As is typically proposed [55], an entropy loss equivalent to two translational degrees of freedom is considered during adsorption for glycerol, acetol, water and hydrogen. Based on the discussion in Section 3.1 it is evident that PG adsorption is weaker than that of glycerol. This is manifested herein as a (slightly) lower loss of translational entropy, see Table 5. Further, due to similarities in the structure of acetol and the partially hydrogenated species, AH in

Table 5

Model parameter estimates, rate and equilibrium coefficients at average temperature, 483 K. Pre-exponential factors, A_{1-7} ($\text{kmol}^{-1} \text{s}^{-1}$) and A_8 (s^{-1}), calculated using transition state theory. ΔS^0 ($\text{J mol}^{-1} \text{s}^{-1}$) calculated from the Sackur–Tetrode equation [54]. E_a (kJ mol^{-1}) and ΔH^0 (kJ mol^{-1}) estimated by regression.

Rate coefficient	A	E_a	k_{483}
k_1^{comp}	10^{15}	$18.5^{\text{a}} \pm 9.2$	$7.8 \times 10^6^{\text{c}}$
k_2^{comp}	10^{13}	$-62.9^{\text{b}} \pm 9.9$	$3.9 \times 10^6^{\text{c}}$
k_3	10^{12}	86.1 ± 11.8	4.9×10^2
k_4	10^{14}	100.2 ± 11.9	1.5×10^3
k_5	10^{13}	87.6 ± 5.1	3.4×10^3
k_6	10^{13}	87.5 ± 4.9	3.4×10^3
k_7	10^{14}	94.5 ± 4.7	6×10^3
k_8	10^{12}	116.4 ± 4.5	0.26
Adsorption coefficients	ΔS^0	$-\Delta H^0$	K_{483}
K_G	-168	65.7 ± 4.4	2.1×10^{-2}
K_A	-166	66.4 ± 1.9	3.2×10^{-2}
K_{PG}	-143	48.1 ± 4.3	5.4×10^{-3}
K_H	-136	55.8 ± 16.1	8.2×10^{-2}
K_{H_2O}	-154	47.3 ± 5.0	1.2×10^{-3}
Equilibrium coefficients	ΔS^0	$-\Delta H^0$	K_{483}
K_{AH}	0	2.4 ± 0.9	1.82
F value		1.5×10^5 ($F_{\text{tab}} : 2.79$)	

^a E_a^{comp} Eq. (35).

^b E_a^{comp} Eq. (36).

^c Non composite i.e., $k_i = A_i \exp(-E_{ai}/RT)$.

reaction (e5), the entropy change during this reaction is assumed to be zero.

The pre-exponential factors, A_i in Eq. (27), are calculated based on the transition state theory [56] see Eq. (28):

$$A = \frac{k_B T}{h} \exp\left(-\frac{\Delta S^\ddagger}{R}\right) \quad (28)$$

with k_B the Boltzmann constant, h the Planck constant and ΔS^\ddagger the entropy difference between reacting species and the transition state. The entropy of a species is related to its mobility, thus based on judicious assumptions on the mobility of the involved species, pre-exponential factors can be a priori calculated. The calculated values also are listed in Table 5. Note that the pre-exponential factors involving glycerol, i.e., k_1, k_4, k_7 are one or two orders of magnitude higher than that involving PG, i.e., k_3, k_5, k_6 . This is in line with the stronger adsorption of glycerol compared to PG, as was apparent from the experimental data analysis. Further, for the production of HPA a scission of the central C–O bond is required, while in the case of acetol formation a scission of terminal C–O bond is required, thus a lower mobility of the transition state for the former reaction (k_7) as compared to the latter (k_1) could be assumed. Finally, due to the relatively higher surface mobility of hydrogen lower pre-exponential factors are obtained for the reactions involving this species, i.e., k_2, k_3, k_4 , see Table 5.

A further reduction in the number of parameters can be achieved through the application of thermodynamic consistency via the production of analogous molecules in the gas phase via a Born–Haber cycle for state functions such as entropy and enthalpy. The thermodynamic consistency applied to reactions 1 and 2 in Fig. 8, see also Table 4, enables the calculation of the surface equilibrium coefficients, K_1 and K_2 , through the following constraints on the parameters:

$$K_1 = \frac{K_A K_{H_2O} K_1^0}{K_G} \quad (29)$$

$$K_2 = \frac{K_{PG} K_2^0}{K_A K_H K_{AH}} \quad (30)$$

The equilibrium coefficient, K_i^0 , is calculated from the Gibbs free reaction energy, $\Delta_r G^0$, with the use of Eqs. (31) and (32).

$$K_i^0 = \exp\left(-\frac{\Delta_r G_i^0}{RT}\right) \quad (31)$$

$$\Delta_r G_i^0 = \Delta_r H_i^0 - T \Delta_r S_i^0 \quad (32)$$

with i representing the reactions 1 and 2 in Fig. 8, $\Delta_r H_i^0$ the standard heat of formation and $\Delta_r S_i^0$ the standard entropy of formation. The data required for the calculation of the standard heat of formation and the standard entropy of formation were acquired from databases such as NIST chemistry webbook [57] and Perry's handbook [58].

Once the pre-exponential factors and equilibrium coefficients have been determined, 14 parameters are left to be estimated by regression, i.e., the 8 activation energies of the surface reactions, E_{ai} , 5 adsorption enthalpies, ΔH_i^0 , and one enthalpy for the surface reaction equilibrium coefficient, K_{AH} . The rate equations derived in this work lead to products of several of these coefficients in the numerator of the resulting equation. In order to limit the correlation between parameters, composite parameters, k_1^{comp} and k_2^{comp} were defined for rate Eqs. (15) and (16). The pre-exponential factors and the entropic contributions were calculated a priori using the previously discussed method. Hence, composite activation energies were estimated via regression:

$$k_1^{\text{comp}} = A_1 \exp\left(-\frac{E_{a1}^{\text{comp}}}{RT}\right) \quad (33)$$

$$k_2^{\text{comp}} = A_2 \exp\left(-\frac{E_{a2}^{\text{comp}}}{RT}\right) \quad (34)$$

with

$$E_{a1}^{\text{comp}} = E_{a1} + \Delta H_G^0 \quad (35)$$

$$E_{a2}^{\text{comp}} = E_{a2} + \Delta H_A^0 + \Delta H_H^0 \quad (36)$$

The parameter estimates as well as the calculated values of the corresponding rate coefficient and the equilibrium constants at average temperature, 483 K, are reported in Table 5. The F value for the global significance of the regression exceeds the tabulated F value by five orders of magnitude implying the global significance of the regression. In addition, each of the individual parameters is estimated significantly, as evident from the narrow 95% probability confidence intervals in Table 5. The maximum value of binary correlation coefficient of 0.986 was obtained between E_{a1}^{comp} and ΔH_G^0 . This value is on the higher side, however, in a catalytic cycle where the surface is nearly saturated by the reactant glycerol, such a value is unavoidable due to the compensating nature of the two parameters. Nevertheless, this correlation is acceptable due to the narrow confidence interval of the estimated parameters, see Table 5.

3.4. Model performance

The parity diagrams for the components involved in the main kinetics and glycerol side reactions are presented in Fig. 9 and those for PG degradation products in Fig. 10. The model calculated molar outlet flow rates for all the components show very good agreement with the experimentally measured molar outlet flow rates, with slight underestimation of ethanol and methanol flow rates.

As evident from the performance curves, i.e. the full lines in Figs. 3–6, the model is capable of adequately reproducing the effect of the operating conditions on the catalytic performance. Eqs. (35) and (36) provide us with values of 84.2 kJ mol^{-1} and 59.3 kJ mol^{-1} for the activation energies of the rate-determining step in the main reactions, E_{a1} and E_{a2} from the estimated composite activation

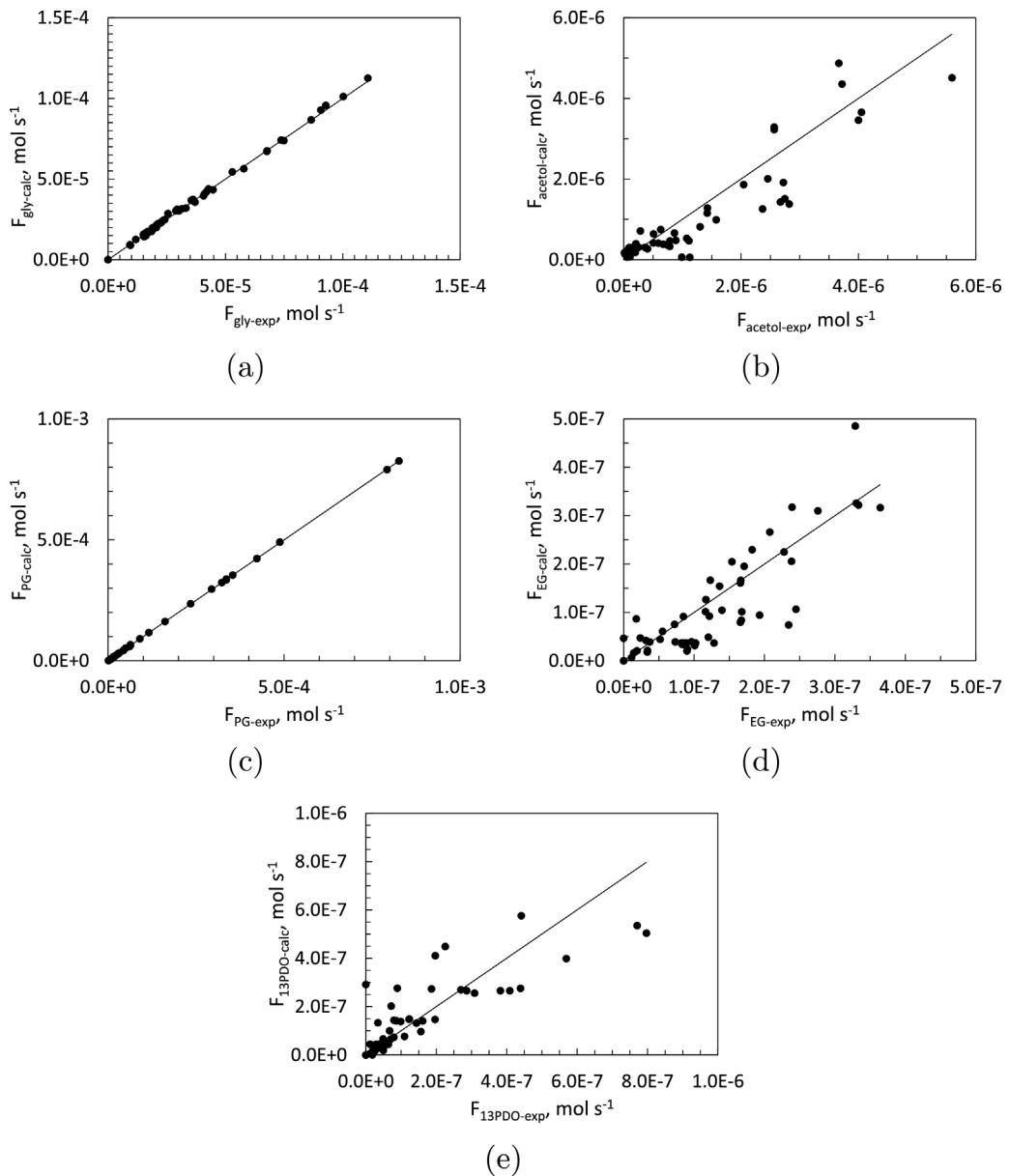


Fig. 9. Parity diagrams for the responses corresponding to the main kinetics and glycerol side reactions: molar flow rate of glycerol (a); acetol (b); propylene glycol (c); ethylene glycol (d); 1,3-propanediol (e). The outlet molar flow rates were calculated using reactor model Eq. (9) along with rate Eqs. (15)–(25) and the parameter estimates from Table 5.

energies E_{a1}^{comp} and E_{a2}^{comp} , see Table 5, respectively. These values are similar to the activation energies of 86.6 kJ mol⁻¹ and 57.8 kJ mol⁻¹ reported by Zhou et al. [28]. The higher activation energy of the first dehydration step explains the experimentally observed more pronounced increase in the dehydration rate with the temperature compared to the hydrogenation rate, see also Fig. 4b. The temperature effect is further enhanced because two adsorption steps are involved in the latter compared to only one in the former, see E_{a1}^{comp} and E_{a2}^{comp} .

The estimated activation energy for the glycerol side reactions towards ethylene glycol and 1,3-propanediol, reactions (4) and (7) in Fig. 8, E_{a4} and E_{a7} amounted to 100.2 kJ mol⁻¹ and 94.5 kJ mol⁻¹ respectively which is 10–15 kJ mol⁻¹ higher than that of the production of acetol from glycerol. Further, the pre-exponential factors for the glycerol side reactions are one order of magnitude lower compared to the dominant dehydration reaction towards acetol. Hence, leading to lower reaction rate coefficients for these

reactions, k_4 and k_7 , explaining the low selectivity towards ethylene glycol and 1,3-propanediol, see Table 5. Less stable transition states for reactions 4 and 7 as compared to reaction 1 explain the higher activation energies for these two reactions. The low selectivity of the PG degradation products 1-propanol, 2-propanol, ethanol and methanol is explained by the coupled effect of lower reaction rate coefficients, k_3 , k_5 and k_6 in Table 5, and the low surface coverage of PG, see Fig. 11. The catalyst surface is typically close to saturation, with glycerol being the most abundant surface species and having a high coverage even at higher conversions. This high glycerol surface coverage explains the low values of apparent glycerol reaction order reported by Vasiliadou and Lemonidou [16] i.e., 0.27 for the consumption of glycerol and 0.17 for the production of PG.

The surface coverages of water and PG, the major products of glycerol hydrogenolysis, are low at lower conversions. As the production of both these products increases with increasing space time the surface coverage of both increases as well. Due to the stronger adsorption PG as compared to water, the PG coverage

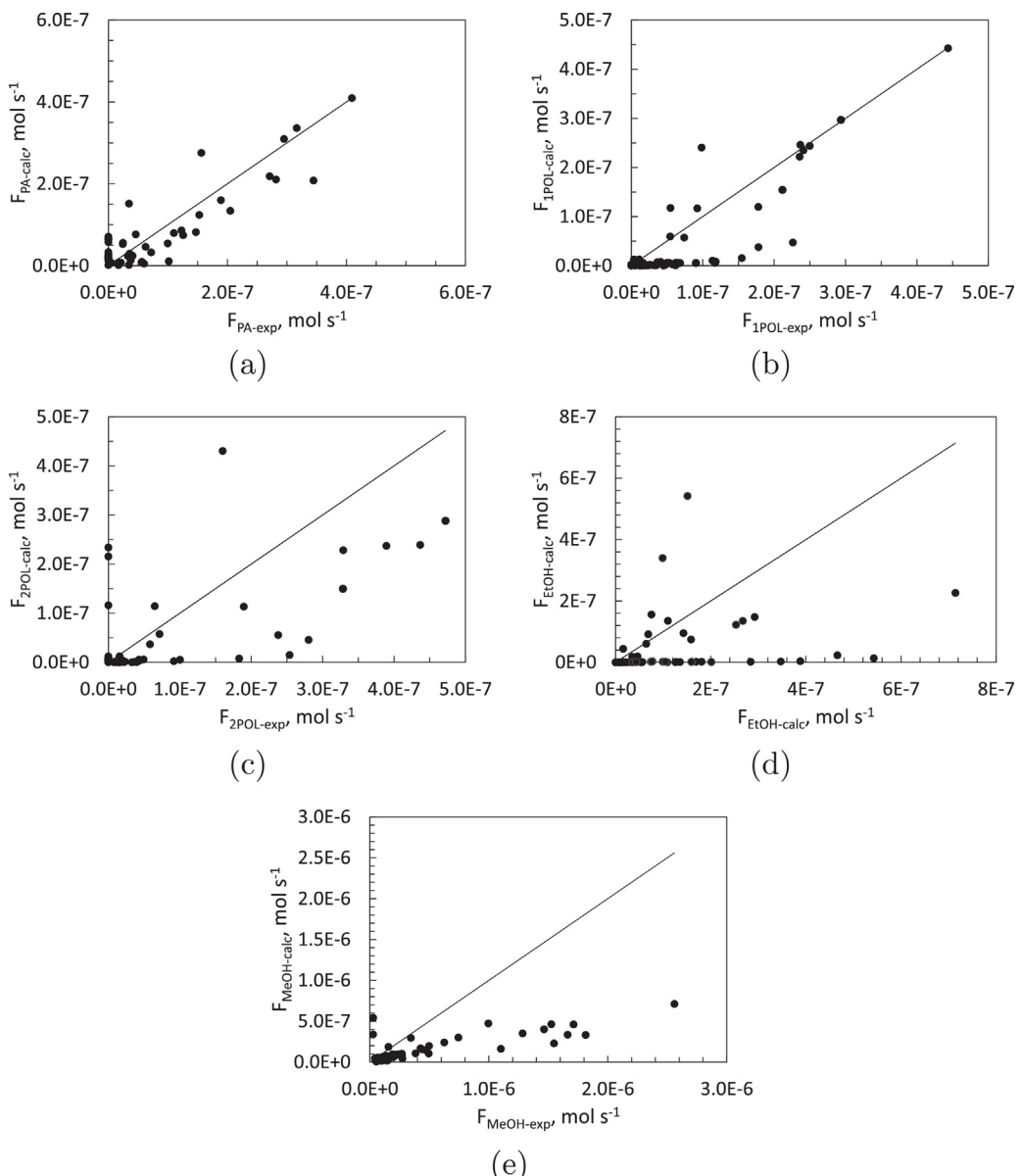


Fig. 10. Parity diagrams for the responses of PG degradation products: molar flow rates of propionic acid (a); 1-propanol (b); 2-propanol (c); ethanol (d); methanol (e). The outlet molar flow rates were calculated using reactor model Eq. (9) along with rate Eqs. (15)–(25) and the parameter estimates from Table 5.

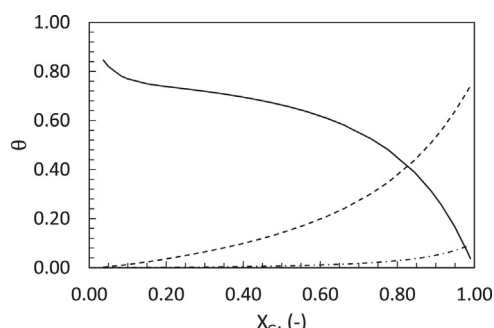


Fig. 11. Calculated surface coverage of different surface species as a function of conversion, $T = 503\text{ K}$, $p = 7.5\text{ MPa}$, $F_{H_2}^0/F_G^0 = 5$. (–) θ_G ; (–) θ_{PG} ; (–·–) θ_{H_2O} using reactor model Eq. (9) along with rate Eqs. (15)–(25) and the parameter estimates from Table 5.

increases faster than that of water with increasing conversion. The low surface coverage of water and PG and the high glycerol surface coverage also explains the minimal effect of product co-feeding on glycerol conversion, as shown in Fig. 6. Similar estimates for the activation energy for PG degradation reaction towards 2-propanone and propanal, reactions (5) and (6) in Fig. 8, suggest similar rates of production for 2-propanol and 1-propanol.

4. Conclusions

A comprehensive kinetic model taking into account the elementary steps for glycerol hydrogenolysis on a supported Cu catalyst has been constructed. The model is able to adequately reproduce the experimental observations in terms of glycerol conversion and product selectivities, both main and the side products, over a wide range of operating conditions.

Glycerol dehydration towards acetol and its further hydrogenation to propylene glycol were found to be the dominant reactions. Glycerol dehydration towards acetol occurs on a larger time scale

than the consecutive conversion of the latter to propylene glycol, allowing high propylene glycol yields from low glycerol conversions onwards. However, this effect is less pronounced with increasing temperature. Both parallel and consecutive side reactions occur at a smaller rate over the entire range of investigated condition. This is caused by the much lower, *i.e.* at least by two order of magnitude, values of the corresponding rate coefficients. The low values of the consecutive reactions can moreover also be attributed to the low adsorption strength of propylene glycol.

Acknowledgements

The research leading to this results has received funding from the Institute for the Promotion of Innovation through Science and Technology in Flanders, IWT and i-CaD the European Research Council under the European Union's Seventh Framework Programme (FP7/2007-2013)/ERC grant agreement 615456. JWT and TR sincerely acknowledge the help of JL in the writing of this work and apologize for any collateral damage caused.

References

- [1] A.J. Ragauskas, C.K. Williams, B.H. Davison, G. Britovsek, J. Cairney, C.A. Eckert, W.J. Frederick, J.P. Hallett, D.J. Leak, C.L. Liotta, J.R. Mielenz, R. Murphy, R. Templer, T. Tschaplinski, *Science* 311 (2006) 484–489.
- [2] E.L. Kunkes, D.A. Simonetti, R.M. West, J.C. Serrano-Ruiz, C.A. Gärtner, J.A. Dumesic, *Science* 322 (2008) 417–421.
- [3] C.S. Wassell Jr., T.P. Dittmer, CSW Jr., T.P. Dittmer, *Energy Policy* 34 (2006) 3993–4001.
- [4] A.E. Atabani, A.S. Silitonga, I.A. Badruddin, T.M.I. Mahlia, H.H. Masjuki, S. Mekhilef, *Renew. Sustain. Energy Rev.* 16 (2012) 2070–2093.
- [5] M.J. Biddy, C.J. Scarlata, C.M. Kinchin, Chemicals from biomass: a market assessment of bioproducts with near-term potential, Technical Report March, National Renewable Energy Laboratory (NREL), Golden, CO, United States, 2016.
- [6] F.H. Reboredo, F. Lidon, F. Pessoa, J.C.J.C. Ramalho, *Trends Biotechnol.* 34 (2016) 3–6.
- [7] M. Pagliaro, R. Ciriminna, H. Kimura, M. Rossi, C. Della Pina, *Angew. Chem. Int. Ed.* 46 (2007) 4434–4440.
- [8] A. Marinas, P. Bruijnincx, J. Frounji, F.J. Urbano, C. Pinel, *Catal. Today* 239 (2015) 31–37.
- [9] Y. Nakagawa, K. Tomishige, *Catal. Sci. Technol.* 1 (2011) 179–190.
- [10] E. Maris, R. Davis, *J. Catal.* 249 (2007) 328–337.
- [11] S. Wang, K. Yin, Y. Zhang, H. Liu, *ACS Catal.* 3 (2013) 2112–2121.
- [12] E.S. Vasiliadou, T.M. Eggenvhuisen, P. Munnik, P.E. de Jongh, K.P. de Jong, A.A. Lemonidou, *Appl. Catal. B* 145 (2014) 108–119.
- [13] E.S. Vasiliadou, E. Heracleous, I.A. Vasalos, A.A. Lemonidou, *Appl. Catal. B* 92 (2009) 90–99.
- [14] C. Montassier, J.C. Ménézo, J. Moukolo, J. Naja, L.C. Hoang, J. Barbier, J.P. Boitiau, *J. Mol. Catal.* 70 (1991) 65–84.
- [15] T. Miyazawa, Y. Kusunoki, K. Kunimori, K. Tomishige, *J. Catal.* 240 (2006) 213–221.
- [16] E. Vasiliadou, A. Lemonidou, *Chem. Eng. J.* 231 (2013) 103–112.
- [17] S. Sato, M. Akiyama, R. Takahashi, T. Hara, K. Inui, M. Yokota, *Appl. Catal. A* 347 (2008) 186–191.
- [18] M.A. Dasari, P.-P. Kiatsimkul, W.R. Sutterlin, G.J. Suppes, *Appl. Catal. A* 281 (2005) 225–231.
- [19] E. van Rynveld, A.S. Mahomed, P.S. van Heerden, M.J. Green, H.B. Friedrich, *Green Chem.* 13 (2011) 1819.
- [20] W. Yu, J. Xu, H. Ma, C. Chen, J. Zhao, H. Miao, Q. Song, *Catal. Commun.* 11 (2010) 493–497.
- [21] A. Marinou, G. Ionita, C.-L. Gáspár, C. Cobzaru, S. Oprea, *React. Kinet. Catal. Lett.* 97 (2009) 315–320.
- [22] M. Balaraju, V. Rekha, P.S. Prasad, B.P. Devi, R. Prasad, N. Lingaiah, *Appl. Catal. A* 354 (2009) 82–87.
- [23] I. Gandarias, P.L. Arias, J. Requies, M.B. Güemez, J.L.G. Fierro, *Appl. Catal. B* 97 (2010) 248–256.
- [24] Z. Huang, F. Cui, H. Kang, J. Chen, X. Zhang, C. Xia, *Chem. Mater.* 20 (2008) 5090–5099.
- [25] L. Guo, J. Zhou, J. Mao, X. Guo, S. Zhang, *Appl. Catal. A* 367 (2009) 93–98.
- [26] E. Vasilidou, A. Lemonidou, *Appl. Catal. A* 396 (2011) 177–185.
- [27] D.G. Lahr, B.H. Shanks, *Ind. Eng. Chem. Res.* 42 (2003) 5467–5472.
- [28] Z. Zhou, X. Li, T. Zeng, W. Hong, Z. Cheng, W. Yuan, *Chin. J. Chem. Eng.* 18 (2010) 384–390.
- [29] A. Torres, D. Roy, B. Subramaniam, R.V. Chaudhari, *Ind. Eng. Chem. Res.* 49 (2010) 10826–10835.
- [30] N. Navidi, J.W. Thybaut, G.B. Marin, *Appl. Catal. A* 469 (2014) 357–366.
- [31] K.V. der Bortgh, K. Toch, V.V. Galvita, J.W. Thybaut, G.B. Marin, *Catalysts* 5 (2015) 1948–1968.
- [32] S. Sie, R. Krishna, *Rev. Chem. Eng.* 14 (1998).
- [33] M.H. Al-Dahhan, M.P. Dudukovii, M.P. Duduković, *AIChE J.* 42 (1996) 2594–2606.
- [34] R.J. Berger, E.H. Stitt, G.B. Marin, F. Kapteijn, J.A. Moulijn, *CATTECH* 5 (2001) 36–60.
- [35] K.M. Ng, *AIChE J.* 32 (1986) 115–122.
- [36] H. Gierman, *Appl. Catal.* 43 (1988) 277–286.
- [37] S.T. Sie, *Rev. Inst. Fr. Pt.* 46 (1991) 501–515.
- [38] J.J. Carberry, *Chemical and Catalytic Reaction Engineering*, McGraw-Hill Chemical Engineering Series, McGraw-Hill, 1976.
- [39] P.B. Weisz, C.D. Prater, *Adv. Catal.* 6 (1954) 60390–60399.
- [40] D.E. Mears, *J. Catal.* 20 (1971) 127–131.
- [41] R.J. Madon, E. Iglesia, *J. Mol. Catal. A: Chem.* 163 (2000) 189–204.
- [42] A. Fredenslund, R.L. Jones, J.M. Prausnitz, *AIChE J.* 21 (1975) 1086–1099.
- [43] T. Holderbaum, J. Gmehling, *Fluid Phase Equilib.* 70 (1991) 251–265.
- [44] J. Gmehling, J. Li, K. Fischer, *Fluid Phase Equilib.* 141 (1997) 113–127.
- [45] R.A. Heidemann, *Fluid Phase Equilib.* 14 (1983) 55–78.
- [46] P.N. Brown, A.C. Hindmarsh, L.R. Petzold, *SIAM J. Sci. Comput.* 15 (1994) 1467–1488.
- [47] H.H. Rosenbrock, *Comput. J.* 3 (1960) 175–184.
- [48] D.W. Marquardt, *J. Soc. Ind. Appl. Math.* 11 (1963) 431–441.
- [49] N.A. Bhore, M.T. Klein, K.B. Bischoff, *Ind. Eng. Chem. Res.* 29 (1990) 313–316.
- [50] A. Bienholz, H. Hofmann, P. Claus, *Appl. Catal. A* 391 (2011) 153–157.
- [51] S. Smeds, D. Murzin, T. Salmi, *Appl. Catal. A* 125 (1995) 271–291.
- [52] J.W. Thybaut, M. Saeyns, G.B. Marin, *Chem. Eng. J.* 90 (2002) 117–129.
- [53] G.B. Marin, G.S. Yablonsky, *Kinetics of Chemical Reactions: Decoding Complexity*, Wiley-VCH Verlag, 2011.
- [54] P. Atkins, J. de Paula, *Atkins' Physical Chemistry*, OUP Oxford, 2010.
- [55] T. Bera, J.W. Thybaut, G.B. Marin, *Ind. Eng. Chem. Res.* 50 (2011) 12933–12945.
- [56] J.A. Dumesic, *The Microkinetics of Heterogeneous Catalysis*, American Chemical Society, 1993.
- [57] P.J.P. Linstrom, W.G. Mallard, *NIST Chemistry WebBook*, 2001.
- [58] R. Perry, D. Green, *Perry's Chemical Engineers' Handbook*, McGraw-Hill Handbooks, McGraw-Hill, 1998.